

Bayesian Recurrent Neural Network Models for Forecasting and Quantifying Uncertainty in Spatial-Temporal Data

Patrick L. McDermott* Christopher K. Wikle

Department of Statistics

University of Missouri

March 29, 2022

Abstract

Recurrent neural networks (RNNs) are nonlinear dynamical models commonly used in the machine learning and dynamical systems literature to represent complex dynamical or sequential relationships between variables. More recently, as deep learning models have become more common, RNNs have been used to forecast increasingly complicated systems. Dynamical spatio-temporal processes represent a class of complex systems that can potentially benefit from these types of models. Although the RNN literature is expansive and thoroughly developed, uncertainty quantification is often ignored. Even when considered, the uncertainty is generally quantified without the use of a rigorous framework, such as a fully Bayesian setting. Here we attempt to

*Department of Statistics, University of Missouri, 146 Middlebush Hall, Columbia, MO 65211 USA;
E-mail: plmyt7@mail.missouri.edu (corresponding author)

quantify uncertainty in a more formal framework while maintaining the forecast accuracy that makes these models appealing, by presenting a Bayesian RNN model for nonlinear spatio-temporal forecasting. Additionally, we make simple modifications to the basic RNN to help accommodate the unique nature of nonlinear spatio-temporal data. The proposed model is applied to a multiscale Lorenz system and to long-lead forecasting of tropical Pacific sea surface temperature.

Keywords: recurrent neural network, Bayesian machine learning, nonlinear dynamical models, long lead forecasting, spatial-temporal

1 Introduction

Nonlinear and quasilinear spatio-temporal data can be found throughout the engineering, biological, geophysical and social sciences. Some examples of such processes include animal or robotic interactions, local economic forecasting, river flow forecasting, visual motion capture, and radar reflectivity precipitation, to name a few. From both a modeling and computational perspective, these types of systems often entail a variety of challenges. While progress has been made with statistical forecasting of univariate nonlinear time-series processes (Fan and Yao, 2005), nonlinear multivariate systems have seen much less progress. Dynamical spatial-temporal models (DSTMs) are multivariate systems that have the added challenge of modeling interactions between different scales of variability while simultaneously facing the curse-of-dimensionality that is exacerbated for nonlinear parametric spatio-temporal models. Both of these issues, along with a need for flexibility, can lead to intense computational demands for nonlinear DSTMs and nonlinear multivariate processes.

Some more recent nonlinear statistical DSTMs include threshold or regime switching models (e.g., Berliner et al., 2000; Wu et al., 2013), general quadratic nonlinear (GQN) models (Wikle and Hooten, 2010), analog models (McDermott and Wikle, 2016), and

mechanistic nonlinear models (Richardson, 2017). While such models have shown success for particular systems, more flexible models are often needed for highly nonlinear systems with complex latent relationships. Furthermore, with only a few exceptions, it can be quite difficult to explicitly specify the nonlinearities in these systems. One exception includes using physically motivated models such as stochastic partial differential equations (e.g., Wikle and Hooten, 2010; Cressie and Wikle, 2011; Richardson, 2017), although this requires some *a priori* knowledge of the dynamics of the system. Due to the many challenges associated with modeling nonlinear spatio-temporal processes, much of the statistical development of these types of models has lagged behind other disciplines such as dynamical systems and machine learning.

One of the many appealing aspects of machine learning methods is their ability to extract salient features and relationships from complex high-dimensional data, particularly for forecasting and classification. The many complex interactions and high-dimensional nature that often define spatio-temporal processes make them a strong candidate for machine learning methods. While there have been past attempts to apply machine learning methods, such as feed-forward neural networks (e.g., Tang et al., 2000), to nonlinear spatial-temporal processes, the explicit accounting for dynamics in these processes has been less of a focus. Moreover, although feed-forward neural networks provide a convenient framework for modeling multivariate processes, they are unable to explicitly capture time-sequential dynamical interactions between variables. As often noted in the dynamical systems literature, explicitly modeling the dynamics is often paramount to successfully forecasting such systems. Recurrent neural networks (RNNs) represent a machine learning model with the potential to effectively model the nonlinear dynamics in multivariate sequential systems such as spatio-temporal processes.

First popularized in the 1980s, RNNs fell out of favor, in part, because of the so-called vanishing gradient problem that makes these models extremely difficult to estimate with

back-propagation. More recently, as deep learning models have gained in popularity, solutions such as the gradient normal clipping strategy proposed in Pascanu et al. (2013) have eased the overall implementation of RNNs. As RNNs have become more manageable from an estimation perspective, they have been increasingly used to model complicated sequential forecasting problems such as visual object tracking (Ning et al., 2016), speech recognition (Yildiz et al., 2013), and text generation (Graves, 2013). Simultaneously, RNNs have also seen a rise in usage in the dynamic systems literature due to their ability to replicate complex attractor dynamics that are often present in chaotic systems (Jaeger, 2001). Thus, RNNs provide a black-box method that can capture dynamical relationships for problems where it is either difficult to specify these relationships *a priori* or little information is available on the specific form of these relationships. Importantly, RNNs fill this void by providing a mechanism for capturing complex sequential relationships between variables, thus providing a modeling tool for a broad set of dynamical problems.

As RNNs have become more prevalent, a variant of the original RNN model, referred to as an echo-state network (ESN) (Lukoševičius and Jaeger, 2009) has become a staple in the dynamical systems literature for solving nonlinear forecasting problems. ESNs are extremely appealing because they retain much of the forecast accuracy of a RNN with a fraction of the computational cost. In essence, ESNs simulate randomly the parameters that make up the hidden states of a RNN (see below), thus reducing the problem to a traditional regression type problem. Although the methodology described here is more within the RNN framework than the ESN, we do borrow and discuss ideas from the ESN literature to motivate choices pertaining to the proposed model. For a spatial-temporal example of an ESN model see McDermott and Wikle (2017).

Despite the broad size and overall scope of the RNN literature, these models are almost always presented without considering uncertainty. The few attempts at quantifying uncertainty are generally presented in an *ad hoc* fashion, without a formal framework. Con-

versely, as previously discussed, the literature on statistical modeling of nonlinear dynamical spatio-temporal systems is relatively sparse, especially compared to its linear counterpart. We address both of these issues by proposing a Bayesian spatial-temporal RNN model, in which the forecasting strength of a traditional RNN is preserved, while also producing comprehensive uncertainty measures. In particular, we introduce a RNN model within a fully Bayesian framework that accounts for uncertainty in both parameters and data in a rigorous fashion. Additionally, we introduce multiple extensions to the traditional RNN model at both the data and latent stage of the model, with the dual aim of facilitating estimation and improving the forecasting ability of the model. The proposed extensions incorporate mechanisms from both the ESN and dynamical systems literature. Furthermore, we regularize the parameters in the model by proposing priors that help deal with over-parameterization, inspired by traditional ESN models.

While others have used Bayesian modeling within the RNN framework (e.g., Chatzis, 2015; Chien and Ku, 2016; Gan et al., 2016), to our knowledge this is the first fully Bayesian RNN trained with traditional Markov Chain Monte Carlo (MCMC) methods. By using MCMC methods, the proposed model and algorithm can more accurately measure uncertainty compared to traditional optimization methods or variational Bayesian methods. Recently, Bayesian methods such as stochastic gradient MCMC (SG-MCMC) have shown promise as an estimation tool for high-dimensional RNNs (i.e., Gan et al., 2016). These stochastic gradient algorithms typically require the partitioning of the data to create so-called mini-batches. Spatio-temporal models often involve explicit dependencies between data points in space and/or time along with hierarchical relationships. Therefore, it may be difficult or impossible to partition the data in this way, which makes such stochastic algorithms prohibitive for many spatial-temporal problems. Similar to traditional RNNs, fitting a RNN within a fully Bayesian framework presents a multitude of computational issues. To assist with computation, we propose using dimension reduction to deal with

high-dimensional spatial-temporal processes. Within a MCMC structure, we borrow the idea of including expansion parameters in the model from the data augmentation literature (e.g., Liu and Wu, 1999; Hobert, 2011), to assist with sampling the highly dependent parameters that make up a RNN.

Section 2 describes the proposed Bayesian spatio-temporal RNN model, along with various modeling details. Next, Section 3 goes through the specifics of the MCMC algorithm developed to implement the model. In the beginning of Section 4 the choices made for the setup of the model are described in detail. Section 4 continues with a simulated multiscale Lorenz model example, followed by a long-lead sea surface temperature forecasting problem. Finally, we end with a concluding discussion on the approach, along with possible future extensions in Section 5.

2 Spatio-Temporal Recurrent Neural Network

2.1 Traditional Recurrent Neural Network

Suppose we are interested in the n_y -dimensional spatial-temporal response \mathbf{Y}_t at time t with corresponding input vector \mathbf{X}_t of dimension n_x , with one being the first value of \mathbf{X}_t as an intercept term. Then the traditional RNN model for multivariate data (e.g., Chung et al., 2015) is defined as follows for $t = 1, \dots, T$:

$$\text{data stage:} \quad \mathbf{Y}_t = g(\mathbf{V}\mathbf{h}_t), \quad (1)$$

$$\text{hidden stage:} \quad \mathbf{h}_t = f(\mathbf{W}\mathbf{h}_{t-1} + \mathbf{U}\mathbf{X}_t), \quad (2)$$

where \mathbf{h}_t is a n_h -dimensional vector of hidden state variables, \mathbf{W} is a square $n_h \times n_h$ weight matrix, \mathbf{U} is a $n_h \times n_x$ weight matrix, and \mathbf{V} is a $n_y \times n_h$ weight matrix. The function $g(\cdot)$ is an activation function that creates a mapping between the response and the hidden states,

while $f(\cdot)$ denotes the activation function for the hidden layer. For a continuous response vector, $g(\cdot)$ is simply the identity function, although this setup can also handle categorical data by allowing $g(\cdot)$ to be the softmax function. Nonlinearity is induced in the RNN model through the form of $f(\cdot)$, which is typically defined as the hyperbolic tangent function (as is assumed throughout this article).

Furthermore, the square weight matrix \mathbf{W} can be thought of analogously to a transition matrix in a typical vector autoregressive (VAR) model. That is, \mathbf{W} models latent dynamic connections between the various hidden states. Thus, underlying nonlinear interactions can effectively be modeled within this framework through \mathbf{W} . Having a mechanism to capture these interactions is often vital when modeling nonlinear spatio-temporal processes (e.g., Wikle, 2015). Overall, the hidden states extract and supply salient hidden dynamic features from the data. Ideally, the hidden states will represent a general set of dynamical patterns from the input data, thus allowing the \mathbf{V} parameters to appropriately weight these patterns. While the RNN defined in (1) and (2) has shown success at forecasting a variety of different systems, the model lacks any explicit error terms, and thus, does not contain a mechanism to formally account for uncertainty in the data, model, or parameters.

2.2 Bayesian Spatio-Temporal Recurrent Neural Network

In this section we introduce the Bayesian spatio-temporal RNN, referred to here after as the BAST-RNN model. Using the same definition for \mathbf{Y}_t as the previous section, the BAST-RNN model is defined as follows:

$$\text{data stage: } \quad \mathbf{Y}_t = \boldsymbol{\mu} + \mathbf{V}_1 \mathbf{h}_t + \mathbf{V}_2 \mathbf{h}_t^2 + \boldsymbol{\epsilon}_t, \quad \boldsymbol{\epsilon}_t \sim \text{Gau}(\mathbf{0}, \mathbf{R}_t), \quad (3)$$

$$\text{hidden stage: } \quad \mathbf{h}_t = f\left(\frac{\delta}{|\lambda_w|} \mathbf{W} \mathbf{h}_{t-1} + \mathbf{U} \widetilde{\mathbf{X}}_t\right), \quad (4)$$

where $\boldsymbol{\mu}$ is a n_y -dimensional spatial intercept vector, \mathbf{V}_1 and \mathbf{V}_2 are each $n_y \times n_h$ output weight matrices, we assume $\mathbf{R}_t \equiv \sigma_c^2 \mathbf{I}$ for all t , and the initial hidden state is set such that $\mathbf{h}_0 \equiv \mathbf{0}$. When necessary, additional temporal or spatial structure can be modeled through the covariance matrix \mathbf{R}_t , although such additional structure is not necessary for the applications presented here. Moreover, λ_w represents the largest eigenvalue of the matrix \mathbf{W} and δ is a scaling parameter with a $\text{Unif}(0, 1)$ prior. By dividing \mathbf{W} by $|\lambda_w|$ and restricting δ , we ensure the spectral radius of \mathbf{W} is at most one. When the spectral radius of \mathbf{W} exceeds one, the model may exhibit chaotic behavior (Lukoševičius and Jaeger, 2009), restricting the spectral radius in this fashion is common in the ESN literature, since \mathbf{W} is not estimated in the ESN model. We find that including δ in the model provides extra flexibility while ensuring the model does not produce chaotic behavior. It's important to note that given the parameters $\delta, \mathbf{W}, \mathbf{U}$, the initial condition \mathbf{h}_0 , and input vectors, $\widetilde{\mathbf{X}}_t$ (see below), the hidden states are known and thus, do not need to be estimated.

Along with scaling \mathbf{W} , we also extend the traditional RNN model by allowing for additional nonlinearity in (3), through $\mathbf{h}_t^2 \equiv (h_{t,1}^2, \dots, h_{t,n_h}^2)'$. By including a nonlinear mapping between the response and \mathbf{h}_t , the proposed model can capture more nonlinear behavior and pickup more extreme intensities (see McDermott and Wikle, 2017). It may also be useful to include higher order interactions between the \mathbf{h}_t 's, although such interactions are not helpful for the applications described below. Next we borrow the idea of embedding the input from the dynamic systems literature as first introduced by Takens et al. (1981), to define the input vector in (4) as:

$$\widetilde{\mathbf{X}}_t' = [\mathbf{X}'_t, \mathbf{X}'_{t-\tilde{\tau}}, \dots, \mathbf{X}'_{t-m\tilde{\tau}}]', \quad (5)$$

where $\tilde{\tau}$ is usually referred to as the embedding lag and m as the embedding length, thus leading to a $(m + 1)n_x$ dimensional input vector (assuming the first element of $\widetilde{\mathbf{X}}_t'$ is an intercept term). By embedding the process of interest the proposed model utilizes all of

the recent trajectory of the system, opposed to a single instance in time. Other statistical nonlinear spatio-temporal forecasting methods (e.g., McDermott and Wikle, 2016, 2017), have shown that embedding the process of interest can lead to more accurate forecasts and more reasonable uncertainty measures.

2.3 BAST-RNN Prior Distributions

The presented BAST-RNN model is comprised of multiple high-dimensional parameter weight matrices, resulting in an over-parameterized model. This problem is not unique to the BAST-RNN, and is often used as a critique on RNNs and feed-forward neural networks in general. Due to the prevalence of this over-parameterization problem, many solutions have been proposed in the machine learning literature. More recently, a method known as dropout (Srivastava et al., 2014) has shown promise as a tool to deal with over-parameterized weight matrices, thereby helping to prevent over-fitting. In essence, dropout creates a type of “hard” regularization by removing entire hidden units (and therefore weight parameters), during training. Similarly, ESN models deal with over-parameterized weight matrices by randomly setting a large percentage of parameters in the weight matrices to zero and then drawing the remaining parameters from a bounded or constrained distribution (see McDermott and Wikle, 2017). These are just two of the many proposed solutions for regularizing the over-parameterized weight matrices that make up neural network models. For statistical models, addressing this problem is similarly vital to helping to prevent over-fitting. Therefore, we proposed regularization priors for the BAST-RNN model (see below) that borrow ideas from both the dropout and ESN method of regularization.

Allowing for many possible sparse networks is a strength of both the dropout and ESN regularization methods. As discussed throughout the Bayesian machine learning literature (e.g., MacKay, 1992; Gan et al., 2016), the natural modeling averaging effect of the fully

Bayesian paradigm acts in a similar way to produce a modeling average effect across many potential networks. Generally in a Bayesian framework, model averaging is induced by using one of the many available priors in the Bayesian variable selection literature (see O’Hara et al., 2009, for an overview). For example, stochastic search variable selection (SSVS) priors (George and McCulloch, 1993) represent an effective tool for shrinking parameter values infinitesimally close to zero. In general, SSVS priors consist of a mixture of two distributions, in which one of the distributions shrinks the parameter value near (or to) zero, while the other distributions allows the parameter to be non-zero.

Although the traditional SSVS prior uses Gaussian distributions (i.e., George and McCulloch, 1997), for the weight matrices \mathbf{W} and \mathbf{U} , we replace the Gaussian distributions with a truncated normal to create a “hard” constraint (see (6) and (7) below). As has been previously noted in the Bayesian neural network literature (i.e., Ghosh et al., 2004), the parameters at the top level of the model (i.e., $\mathbf{V}_1 \mathbf{h}_t$ and $\mathbf{V}_2 \mathbf{h}_t^2$ for the BAST-RNN model in (3)) are not identifiable. By using truncated normal distributions, we are in a broad sense constraining the contribution of each weight matrix \mathbf{W} and \mathbf{U} towards the \mathbf{h}_t ’s, and thus, the values of the \mathbf{h}_t ’s. While helping to partly alleviate this identifiability problem, we also find that using truncated normals helps improve mixing when performing MCMC estimation. Finally, as discussed in Ghosh et al. (2004), this non-identifiability is not an issue when parameters are given proper priors and interest is only in prediction, as is the case here.

Using the SSVS framework described above, each element of the weight matrix $\mathbf{W} = [w_{i,\ell}]$ is given the following prior distribution:

$$w_{i,\ell} = \gamma_{i,\ell}^w \text{TN}_{[-a_w, a_w]}(0, \sigma_{w,0}^2) + (1 - \gamma_{i,\ell}^w) \text{TN}_{[-a_w, a_w]}(0, \sigma_{w,1}^2), \quad (6)$$

where $\sigma_{w,0}^2 \gg \sigma_{w,1}^2$ and the notation $\text{TN}_{[-a_w, a_w]}$ denotes a truncated normal distribution, truncated between $-a_w$ and a_w . Moreover, $\gamma_{i,\ell}^w$ represents an indicator variable with prior,

$\gamma_{i,\ell}^w \sim \text{Bernoulli}(\pi_w)$, such that π_w can be thought of as the prior probability of including $w_{i,\ell}$ in the model. An analogous prior is used with each element of $\mathbf{U} = [u_{i,r}]$ for $r = 1, \dots, (m+1)n_x$, such that:

$$u_{i,r} = \gamma_{i,r}^u \text{TN}_{[-a_u, a_u]}(0, \sigma_{u,0}^2) + (1 - \gamma_{i,r}^u) \text{TN}_{[-a_u, a_u]}(0, \sigma_{u,1}^2), \quad (7)$$

where $\gamma_{i,r}^u \sim \text{Bern}(\pi_u)$ and $\sigma_{u,0}^2 \gg \sigma_{u,1}^2$. As described in Section 4.1, both hyper-parameters π_w and π_u are set to small values to regularize many of the parameters in the model (since $\sigma_{w,1}^2$ and $\sigma_{u,1}^2$ are set to very small values, as detailed in Appendix A). The priors defined in (6) and (7) mimic aspects of the regularization produced from using dropout or the ESN model by similarly removing or (nearly) zeroing out many of the model parameters. While developing the proposed model we also considered other popular Bayesian variable selection priors such as the Lasso prior (Park and Casella, 2008) and the horseshoe prior (Carvalho et al., 2010). We found the proposed SSVS priors provided the most flexibility with our approach.

Next, the parameters matrices \mathbf{V}_1 and \mathbf{V}_2 are given traditional SSVS priors with Gaussian distributions (see Appendix A for the full details). Although a $L2$ (ridge) penalty is typically used for estimating the \mathbf{V} matrices in the ESN model, we found this penalty to be overly restrictive for the BAST-RNN model. To finish the specification of the model, the spatial intercept is given the Gaussian prior, $\boldsymbol{\mu} \sim \text{Gau}(\mathbf{0}, \sigma_\mu^2 \mathbf{I})$, and the variance parameter σ_ϵ^2 is given the inverse-gamma prior, $\sigma_\epsilon^2 \sim \text{IG}(\alpha_\epsilon, \beta_\epsilon)$. See Appendix A for the specific values of the hyper-parameters presented in this section.

2.4 Dimension reduction

With the rise of machine learning and high-dimensional methods has also come the increase in size of spatio-temporal data sets. In general, although not always, this increase in

size can be attributed to the number of spatial locations (or grid-points) in a given data set. When n_y or n_x (or both) is large, the BAST-RNN model can quickly become computationally prohibitive. For example, with more locations, each step of the MCMC algorithm (in particular the Metropolis-Hastings steps) will become more computationally costly. Secondly, with more locations it may be necessary to increase the value of n_h , thus increasing the size of all the weight parameter matrices in the model. A common solution to this problem in the spatio-temporal dynamical modeling literature is to use some form of dimension reduction (i.e., Cressie and Wikle, 2011), which is often justified since the underlying dynamics typically live in a lower dimensional manifold than the data.

There is a great deal of flexibility when selecting a dimension reduction method for high-dimensional spatio-temporal processes. Depending on the application, any number of methods can be selected from linear methods such as wavelets, splines, or principal components, or nonlinear methods such as Laplacian eigenmaps (Belkin and Niyogi, 2001), restricted Boltzmann machines (Nair and Hinton, 2010), or diffusion maps (Coifman and Lafon, 2006), just to name a few. To describe how dimension reduction can be used with the BAST-RNN model, suppose we let \mathbf{Z}_t be a n_z -dimensional observed response vector at time t . Then \mathbf{Z}_t can be decomposed such that $\mathbf{Z}_t \approx \Phi \mathbf{Y}_t$, where Φ is a $n_z \times n_b$ basis function matrix and \mathbf{Y}_t is a n_b -dimensional vector of basis coefficients. Importantly, we assume that $n_b \ll n_z$, thus, \mathbf{Y}_t provides a lower-dimensional set of variables (expansion coefficients) with which our model can be built. For example, the proposed BAST-RNN model can be re-formulated using the basis coefficients as follows:

$$\text{data model:} \quad \mathbf{Z}_t = \Phi \mathbf{Y}_t + \boldsymbol{\nu}_t \quad \boldsymbol{\nu}_t \sim \text{Gau}(\mathbf{0}, \Sigma_\nu), \quad (8)$$

$$\text{process model:} \quad \mathbf{Y}_t = \boldsymbol{\mu} + \mathbf{V}_1 \mathbf{h}_t + \mathbf{V}_2 \mathbf{h}_t^2 + \boldsymbol{\epsilon}_t \quad \boldsymbol{\epsilon}_t \sim \text{Gau}(\mathbf{0}, \mathbf{R}_t), \quad (9)$$

where the error term $\boldsymbol{\nu}_t$ helps account for the truncated error caused by using a reduced dimension. For some applications it may be more important than others to include the

error term (i.e., ν_t) in (8). Although the applications examined below do not include this truncation error term, the proposed framework allows for the potential to account for such uncertainty.

3 Parameter Expansion MCMC

Similar to non-Bayesian RNN estimation, the nonlinearity and dependence structures in the BAST-RNN model present unique estimation and computational issues. Both the \mathbf{W} and \mathbf{U} weight matrices in the BAST-RNN model are particularly difficult to estimate due to the fact both are within the nonlinear activation function, along with the many dependencies that exist between these two matrices. This dependence occurs since, given the embedded input ($\widetilde{\mathbf{X}}_t$ above) and δ , the hidden states in (4) are completely determined by \mathbf{W} and \mathbf{U} . Thus, as \mathbf{W} and \mathbf{U} change, so do the values of the hidden states. Importantly, since \mathbf{W} weights the hidden states, the parameter values of \mathbf{W} are highly dependent on the specific values of the hidden states and by proxy the values of \mathbf{U} .

Parameter expansion data augmentation (PXDA) (e.g., Liu and Wu, 1999; Hobert, 2011) is a method developed for missing data problems in which mixing for MCMC algorithms is difficult due to dependence between parameters. While the parameter expansion in the PXDA algorithm is generally applied to missing data, we borrow the parameter expansion idea and apply it to the sampling of the \mathbf{W} matrix (we did not find it necessary to use this same technique on the \mathbf{U} matrix). In essence, parameter expansion MCMC (PX-MCMC) introduces extra parameters (referred to as the expansion parameters) into the model to create extra randomness. For example, suppose for a given iteration of the MCMC algorithm we sampled \mathbf{W} and then \mathbf{U} . Instead of moving from \mathbf{W} to \mathbf{U} (i.e., $\mathbf{W} \rightarrow \mathbf{U}$), the expanded parameter is used to create an intermediate step such that $\mathbf{W} \rightarrow \mathbf{W}' \rightarrow \mathbf{U}$. That is, \mathbf{W}' is a randomly transformed version of \mathbf{W} , thus helping to break some of the dependence between weight matrices \mathbf{W} and \mathbf{U} . Without this extra randomness, the samples

for the weight matrices \mathbf{W} and \mathbf{U} quickly become degenerate.

By introducing this intermediate step, the mixing in the MCMC algorithm greatly improves for both the \mathbf{W} and \mathbf{U} matrix. The amount of randomness used to transform \mathbf{W} into \mathbf{W}' can be thought of similarly to the learning rate parameter used in traditional stochastic gradient descent (SGD) or SG-MCMC algorithms for machine-learning problems. Typically, a learning rate parameter is used in SGD algorithms to determine how fast or slow the weights in a given model are learned. For example, in the SG-MCMC algorithm developed in Gan et al. (2016), at each iteration when the model parameters are updated a standard multivariate Gaussian distribution multiplied by a learning rate parameter is added to the updated parameter values. Similarly to the learning rate for SGD, this extra randomness allows the algorithm to better search the entire parameter space, thus improving the mixing of the algorithm. To more rigorously describe the PX-MCMC algorithm, we need to define additional notation.

Suppose we introduce the expansion parameter matrix α , where $\alpha = [\alpha_{i,\ell}]$ for $i = 1, \dots, n_h$ and $\ell = 1, \dots, n_h$, and $\alpha \subset \mathbf{A}$, where $\mathbf{A} \in \mathbb{R}^{n_h^2}$. Next, we define the transformation $t_\alpha : \mathbf{W} \rightarrow \mathbf{W}$, where we require t_α to be a one-to-one differentiable function and denote the Jacobian for this transformation as $J_\alpha(\mathbf{W})$. Next, let $\Gamma_{V_1}, \Gamma_{V_2}, \Gamma_U$, and Γ_W denote all of the indicator functions for the SSVS priors corresponding to the respective weight matrices in (3) and (4). We define Θ as all of the parameters in the model not associated with \mathbf{W} , such that $\Theta \equiv \{\mathbf{V}_1, \mathbf{V}_2, \boldsymbol{\mu}, \Gamma_{V_1}, \Gamma_{V_2}, \mathbf{U}, \Gamma_U, \delta, \sigma_\epsilon^2\}$. Finally, let $\mathbf{Y}_{1:T} \equiv \{\mathbf{Y}_1, \dots, \mathbf{Y}_T\}$ and $\tilde{\mathbf{X}}_{1:T} \equiv \{\tilde{\mathbf{X}}_1, \dots, \tilde{\mathbf{X}}_T\}$, with the notation $[\cdot]$ denoting a distribution, and we define the likelihood of the model (before the introduction of the expansion parameter matrix α) using the following slight abuse of notation
$$\prod_{t=1}^T [\mathbf{Y}_t \mid \Theta, \mathbf{W}, \Gamma_W, \tilde{\mathbf{X}}_t] = [\mathbf{Y}_{1:T} \mid \Theta, \mathbf{W}, \Gamma_W, \tilde{\mathbf{X}}_{1:T}].$$

Algorithm 1 PX-MCMC algorithm

1. Sample $[\mathbf{W}, \Gamma_W] \sim [\mathbf{W}, \Gamma_W \mid \Theta, \mathbf{Y}_{1:T}, \tilde{\mathbf{X}}_{1:T}]$.
 2. Generate $\alpha_{0,i,\ell} \sim \text{Gau}(0, \sigma_\alpha^2)$ for $i = 1, \dots, n_h$ and $\ell = 1, \dots, n_h$.
 3. Transform $\tilde{\mathbf{W}} = t_{\alpha_0}^{-1}(\mathbf{W})$.
 4. Sample $[\alpha \mid t_\alpha(\tilde{\mathbf{W}}), \Gamma_W, \Theta, \mathbf{Y}_{1:T}, \tilde{\mathbf{X}}_{1:T}] \propto$
 $[\mathbf{Y}_{1:T} \mid t_\alpha(\tilde{\mathbf{W}}), \Gamma_W, \Theta, \alpha, \tilde{\mathbf{X}}_{1:T}] [t_\alpha(\tilde{\mathbf{W}}) \mid \Gamma_W, \alpha] [\alpha] |J_\alpha(\tilde{\mathbf{W}})|$.
 5. Set $\mathbf{W}^* = t_\alpha(\tilde{\mathbf{W}}) = t_\alpha(t_{\alpha_0}^{-1}(\mathbf{W}))$.
 6. Sample $\Theta \sim [\Theta \mid \mathbf{W}^*, \mathbf{Y}_{1:T}, \tilde{\mathbf{X}}_{1:T}]$.
-

Now, we outline the PX-MCMC for the BAST-RNN model; note, we leave the detailed derivations of the presented algorithm for the Appendix. Using the notation defined above, one can show the following relationship for the joint posterior of \mathbf{W} and Γ_W :

$$[\mathbf{W}, \Gamma_W \mid \Theta, \mathbf{Y}_{1:T}, \tilde{\mathbf{X}}_{1:T}] = \int_{\mathbf{A}} [t_\alpha(\mathbf{W}), \Gamma_W \mid \Theta, \mathbf{Y}_{1:T}, \tilde{\mathbf{X}}_{1:T}] |J_\alpha(\mathbf{W})| [\alpha] d\alpha. \quad (10)$$

To sample from the integral in (10), we assume $[\mathbf{W}', \Gamma_W] \sim [t_\alpha(\mathbf{W}), \Gamma_W \mid \Theta, \mathbf{Y}_{1:T}, \tilde{\mathbf{X}}_{1:T}]$ and $\alpha_0 \sim [\alpha]$. We will take $\mathbf{W} = t_{\alpha_0}^{-1}(\mathbf{W}')$ by using a change-of-variable, thus resulting in the joint sampling of \mathbf{W} and Γ_W . For the BAST-RNN model implementation we use the Gaussian distribution $\text{Gau}(\mathbf{0}, \sigma_\alpha^2 \mathbf{I})$ for $[\alpha]$, where the prior variance σ_α^2 can be thought of similarly to the learning rate parameter used in many machine learning estimation algorithms. There is a great deal of flexibility with regards to the particular distribution use for $[\alpha]$ (i.e., Hobert, 2011) and its choice should depend on the particular model and applica-

tion. Letting $\widetilde{\mathbf{W}} \equiv t_{\alpha_0}^{-1}(\mathbf{W})$, we can sample Θ using the following:

$$\begin{aligned}
& [\Theta, \boldsymbol{\alpha} \mid \mathbf{W}, \boldsymbol{\Gamma}_W, \mathbf{Y}_{1:T}, \widetilde{\mathbf{X}}_{1:T}] \propto \\
& [\mathbf{Y}_{1:T} \mid t_{\boldsymbol{\alpha}}(\widetilde{\mathbf{W}}), \boldsymbol{\Gamma}_W, \Theta, \boldsymbol{\alpha}, \widetilde{\mathbf{X}}_{1:T}] [\Theta \mid t_{\boldsymbol{\alpha}}(\widetilde{\mathbf{W}}) \mid \boldsymbol{\Gamma}_W, \boldsymbol{\alpha}] [\boldsymbol{\alpha} \mid J_{\boldsymbol{\alpha}}(\widetilde{\mathbf{W}})]. \quad (11)
\end{aligned}$$

Taking (10) and (11) together, we can form the PX-MCMC algorithm seen in Algorithm 1. For the sake of brevity, we leave the specific full-conditional distribution for all of the model parameters for the Appendix.

4 Applications

We begin by discussing the specifics of implementing the model, including, comparison metrics and methods, the MCMC setup, and specific hyper-parameter choices. We then detail the analysis of a simulated multiscale Lorenz data set. Finally, the setup and results of a Pacific sea surface temperature (SST) long-lead forecasting application are described.

4.1 Model setup

Since the stated goal of developing the BAST-RNN model is to produce accurate forecasts with realistic uncertainty bounds, we evaluate the model in terms of both mean squared prediction error (MSPE) and continuous ranked probability score (CRPS). Both measures are only calculated for out-of-sample values, since the focus of the proposed model is on forecasting. For our purposes, the MSPE is defined as the average squared difference between the out-of-sample forecasts and true out-of-sample values across all time periods and spatial locations. Moreover, for a predictive CDF F and true out-of-sample realization

h , CRPS is defined as (i.e., Matheson and Winkler, 1976):

$$\text{CRPS}(F, h) = \int_{\mathbb{R}} (F(r) - \mathbb{1}\{r \geq h\})^2 dr. \quad (12)$$

The usefulness of CRPS lies in its ability to both quantify the accuracy and distribution of a forecast, thus producing a quantifiably measure of how well a model quantifies uncertainty (i.e., Gneiting and Katzfuss, 2014). In all the applications presented below, after the model is trained on the in-sample data, out-of-sample forecasts are made successively at the given lead time for a particular application. We define lead time as the temporal difference between the input and the response. These successive forecasts are made by repeatedly plugging in the inputs for a given lead time to get out-of-sample forecasts, using the posterior samples from the BAST-RNN.

For the sake of comparison, we also evaluated the ensemble quadratic ESN (E-QESN) model from McDermott and Wikle (2017) for all of the applications below. The E-QESN model presents a strong comparison model since it can also quantify uncertainty and shares much of the same flexibility as the BAST-RNN model. Few other methods share the E-QESN’s ability to produce forecasts with uncertainty quantification at such a low computational and implementation cost.

Next, we compared to a model referred to as the linear DSTM, defined as:

$$Y_{t,i} = \sum_{j=1}^{n_y} a_{ij} Y_{t-1,j} + \zeta_{t,i}^{(l)}, \quad (13)$$

for each location $Y_{t,i}$, where $\{a_{i,j}\}$ are weight parameters and $\zeta_{t,i}^{(l)} \sim \text{Gau}(0, \sigma_{\zeta_l}^2)$. Finally, we also compare to the GQN model discussed above (Wikle and Hooten, 2010). For the results presented below, the GQN model is defined as:

$$Y_{t,i} = \sum_{j=1}^{n_y} a_{ij} Y_{t-1,j} + \sum_{k=1}^{n_y} \sum_{\ell=1}^{n_y} b_{i,k,\ell} Y_{t-1,k} Y_{t-1,\ell} + \zeta_{t,i}^{(q)}, \quad \zeta_{t,i}^{(q)} \sim \text{Gau}(0, \sigma_{\zeta_q}^2). \quad (14)$$

Although both the GQN and linear DSTM can be formulated as Bayesian models, such formulations are not pursued here. While this is not an exhaustive list of comparison methods, these methods represent much of the state-of-the art in statistical spatial-temporal modeling and nonlinear spatial-temporal forecasting.

For the remainder of this section we discuss the details of implementing the BAST-RNN model. Note, the implementation settings discussed here are used for all of the presented applications. The BAST-RNN model is implemented using the PX-MCMC algorithm (Algorithm 1), sampling 100,000 iterations with the first 25,000 iterations treated as burn-in. The number of hidden units (n_h) is set to 20. We found this number of hidden units balanced computational cost and forecast accuracy in that larger numbers of hidden units produced similar results in terms of forecast accuracy, but substantially slowed the algorithm. Although not pursued here, the number of hidden units could be varied by using advanced computational methods such as reversible jump MCMC (Green, 1995). Selection of the parameters for the embedded input, defined in (5), is conducted by using cross-validation, over an application specific grid with the E-QESN model (see McDermott and Wikle, 2017, for a detailed description of this procedure). As suggested by Lukoševičius (2012), both the input and response are scaled by their respective means and standard deviations.

While we leave the specific hyper-parameter values used in the prior distributions to the Appendix, we will briefly discuss the more important of these choices. Regarding the parameter weight matrices that make up the hidden units (i.e., \mathbf{W} and \mathbf{U}), the hyper-parameters π_w and π_u (as defined in Section 2.3) are set to small values to encourage sparseness and prevent overfitting. In particular, these hyper-parameters are set such that $\pi_w > \pi_u$, since the matrix \mathbf{U} is weighting the data; we found this specification helped prevent overfitting to the in-sample data. Moreover, a_w and a_u are both set to small values so that $a_w = a_u$, as to follow the common practice in machine learning of bounding parameter values to prevent overfitting (i.e., Lukoševičius, 2012).

4.2 Multiscale Lorenz-96 Model

Many RNN methods in the literature use the classic three-variable Lorenz model from Lorenz (1963) to evaluate forecasting ability (e.g., Ma et al., 2007; Chandra and Zhang, 2012). Due to the chaotic and nonlinear behavior of the Lorenz model, this system produces data resembling a realistic nonlinear forecasting problem. Here, evaluation of the BAST-RNN model is applied to the less cited, but more spatially interesting Lorenz model (Lorenz, 1996), often referred to as the Lorenz-96 model, which explicitly includes spatial locations and structure. An extension of the Lorenz-96 model, the *multiscale Lorenz-96* model contains interacting large-scale and small-scale processes, where the large-scale locations are directly influenced by neighboring small-scale locations and vice-versa (Wilks, 2005; Chorin and Lu, 2015; Grooms and Lee, 2015). We consider this multiscale Lorenz-96 model here.

While multiple parameterizations exist for the multiscale Lorenz-96 model, we use the following parameterization from Chorin and Lu (2015), (note, the superscript L is used throughout to signify variables from the Lorenz-96 model):

$$\begin{aligned}\frac{dx_{k_L}^L}{dt} &= x_{k_L-1}^L(x_{k_L+1}^L - x_{k_L-2}^L) - x_{k_L}^L + \tilde{F} + \frac{h_x}{J_L} \sum_{j_L} y_{j_L, k_L}^L + \eta_{k_L}^{(1)}, \\ \frac{y_{j_L, k_L}^L}{dt} &= \frac{1}{\epsilon_L} [y_{j_L+1, k_L}^L (y_{j_L-1, k_L}^L - y_{j_L+2, k_L}^L) - y_{j_L, k_L}^L + h_y x_{k_L}^L],\end{aligned}\quad (15)$$

for $j_L = 1, \dots, J_L$ and $k_L = 1 \dots, K_L$. For notational convenience the subscript t has been suppressed from (15). The state variable $x_{k_L}^L$ denotes a large-scale process location, with each large-scale location having J_L corresponding small-scale locations denoted by y_{j_L, k_L}^L . Each of the large-scale locations can be thought of as equally spaced spatial variables on a one-dimensional circular spatial domain such that $x_{K_L+1}^L = x_1^L$ (i.e., periodic boundary conditions). A given set of small-scale locations corresponding to a particular large-scale location, is defined with a similar spatial domain and boundary condition.

Furthermore, the parameter \tilde{F} in (15) denotes a forcing parameter, while ϵ_L controls the time-scale separation between the large and small-scale locations, $\eta_{k_L}^{(1)}$ is an additive Gaussian noise term such that $\eta_{k_L}^{(1)} \sim \text{Gau}(0, \sigma_{\eta_1}^2)$, with $\sigma_{\eta_1}^2 = 1$, and h_x, h_y control how much the large and small-scale locations influence each other, respectively. For the analysis using the BAST-RNN model, we simulate from the full model but treat the small-scale locations as unobserved and evaluate the BAST-RNN only on the large-scale locations, thus creating a difficult but reasonable nonlinear spatio-temporal forecasting problem. After burn-in, 400 time periods are retained from the the multiscale Lorenz-96 model, with the last 75 time periods treated as out-of-sample. The data are simulated with a time step of $\Delta = .05$ by using an Euler solver. We use the same parameter values as Chorin and Lu (2015) to simulate the data such that: $K_L = 18, J_L = 20, \tilde{F} = 10, \epsilon_L = 0.5, h_x = -1$, and $h_y = 1$. In order to create a more realistic statistical forecasting problem, Gaussian white noise error is added to each large-scale realization, so that $z_{k_L}^L = x_{k_L}^L + \eta_{k_L}^{(2)}$, where $\eta_{k_L}^{(2)} \sim \text{Gau}(0, \sigma_{\eta_2}^2)$, with $\sigma_{\eta_2}^2 = (2.5)^2$. The forecasting problem is made slightly more nonlinear by setting the lead time to three periods (i.e., the input and response are separated by three periods). Along with using the implementation settings detailed in Section 4.1, for the embedded input the following parameters are used: $\tilde{\tau} = 2$ and $m = 4$.

Posterior mean forecasts and prediction intervals (P.I.s) for the BAST-RNN model with the multiscale Lorenz-96 data can be seen for six locations in Figure 1. Note that because a high signal-to-noise ratio was used to simulate the data, the true signal is substantially corrupted by the additive noise. Generally, the multiscale Lorenz-96 model is analyzed as a more smooth process with much less additive noise than the data simulated in Figure 1. Despite the high level of noise, the model picks up much of the signal for the six locations shown in Figure 1. Moreover, it appears that many of the true values of the process are captured by the 95% P.I.s. Across all 18 large-scale locations in the simulated data, 94.96% of the true values are contained within the 95% P.I.s, while only 86.37% of the true values

are contained within the intervals produced by the E-QESN model.

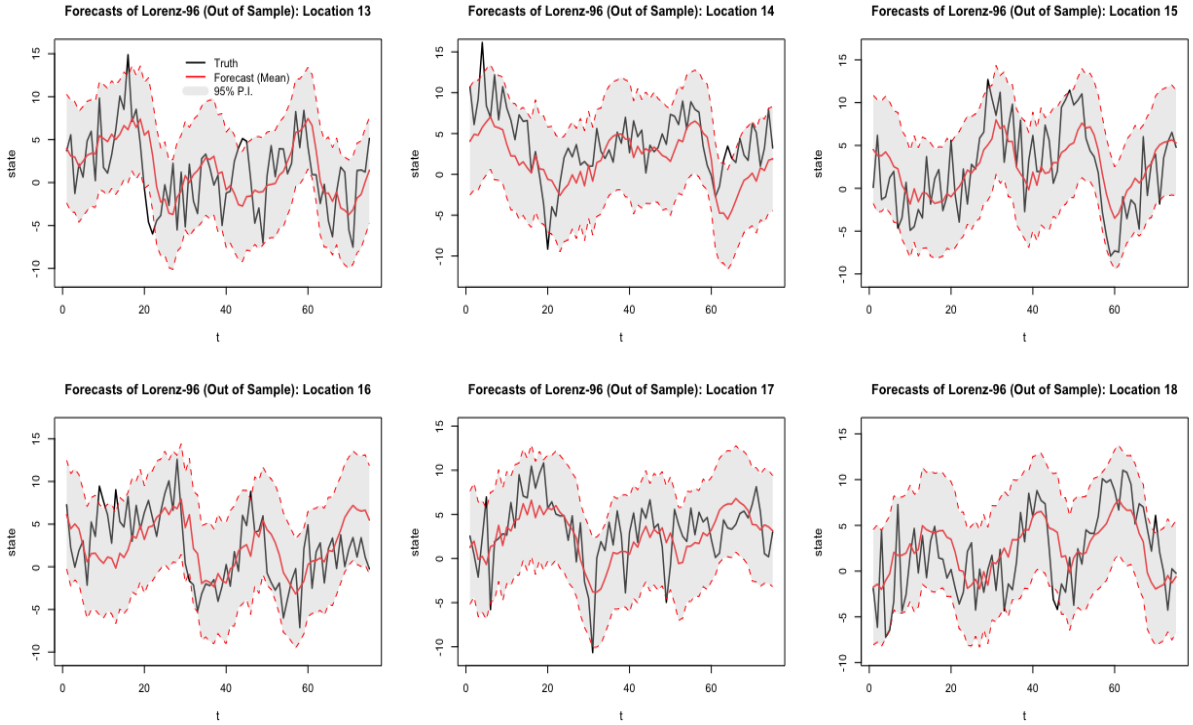


Figure 1: Posterior out-of-sample summaries for 6 of the 18 large-scale locations from the simulated multi-scale Lorenz-96 data over 75 periods. The black line in each plot represents the true simulated value, while the red line denotes the forecasted posterior mean from the BAST-RNN model. For each plot, the shaded grey area signifies the 95% posterior prediction intervals.

A more detailed comparison of the BAST-RNN model and the models described in Section 4.1 can be found in Table 1. With regards to MSPE, Table 1 shows the BAST-RNN outperforming the other 3 competing models by producing lower values. It's not entirely surprising, considering the level of nonlinearity in the simulated data, that the BAST-RNN and E-QESN model outperformed the other two less flexible models. Compared to the E-QESN model, Table 1 also shows the BAST-RNN model produces superior uncertainty measures by having a lower CRPS. Overall, these results simultaneously demonstrate the ability of the BAST-RNN model to accurately forecast the trend in a nonlinear process, while also giving robust measures of uncertainty.

Model	MSPE	CRPS
BAST-RNN	13.61	158.24
E-QESN	13.99	166.34
GQN	14.86	-
Lin. DSTM	15.12	-

Table 1: Comparison for the 4 forecasting methods for the simulated multiscale Lorenz-96 data in terms of mean squared prediction error (MSPE). The column labeled CRPS (continuous ranked probability score) shows results for the BAST-RNN and E-QESN model only. Both metrics are calculated over all out-sample periods and locations.

4.3 Long-lead Tropical Pacific SST Forecasting

Tropical Pacific sea surface temperature (SST) is one of the largest sources of variability affecting global climate. Changes in SST at various time-scales contribute to extreme weather events across the globe, from hurricanes to severe droughts. Therefore, accurate long-lead SST forecasts are vital for many resource managers. With regards to SST, of particular interest is the anomalous warming (El Niño) and cooling (La Niña) of the Pacific ocean, referred to collectively as the El Niño Southern Oscillation (ENSO) phenomena.

The focus of our analysis is on the ENSO phenomena that occurred during 2015 and 2016. Besides being one of the most extreme ENSO events on record, many forecasting methods that were effective for past ENSO cycles failed to accurately forecast the 2015-2016 cycle (i.e., L’Heureux et al., 2016; Hu and Fedorov, 2017). As described in Barnston et al. (2012), there are currently a suite of both deterministic and statistical methods for forecasting SST, with the statistical models often doing as good or better than the deterministic models. A summary of the deterministic models used to forecast SST can be found in works such as Barnston et al. (1999) and Jan van Oldenborgh et al. (2005). Some nonlinear statistical models that have shown success for the ENSO forecasting problem include the general quadratic nonlinear (GQN) model (i.e., Wikle and Hooten, 2010), the

switching Markov model (Berliner et al., 2000), and classic neural network models (i.e., Tangang et al., 1998). It is important to note that to our knowledge, this is the first machine learning method applied to the ENSO forecasting problem with a formal mechanism for quantifying uncertainty. The BAST-RNN model is used to produce out-of-sample forecasts with a lead time of six months for the 2015-2016 ENSO cycle. Due to the lead time and intensity of the 2015-2016 ENSO cycle, this presents a difficult nonlinear forecasting problem.

The SST forecasting application uses monthly data over a spatial domain covering 29°S-29°N latitude and 124°E-70°W longitude, with a resolution of $2^\circ \times 2^\circ$, leading to 2,229 oceanic spatial locations. The data set comes from the publicly available extended reconstruction sea surface Temperature (ERSST) data (<http://iridl.ldeo.columbia.edu/SOURCES/.NOAA/>) provided by national ocean and atmospheric administration (NOAA) and covers a period from 1970 through 2016. As is common in the climatology literature, the SST data are converted into anomalies by subtracting the monthly climatological means calculated over the period 1981–2010, for each spatial location. Furthermore, when constructing ENSO forecasting methods, it is common to evaluate the performance of a given method using the univariate summary measure for ENSO referred to as the Niño 3.4 index. Much of the variability in the ENSO phenomena is contained in the Niño 3.4 region (i.e., 5°S-5°N, 120°-70°W), so for our purposes, the Niño 3.4 index is simply the average SST anomaly over all locations in the this region for a given month (see Figure 3).

Training of the model is implemented using Algorithm 1 and the setup from Section 4.1 with data from January 1970-August 2014, while out-of-sample forecasts were made every two months for a period from February 2015-December 2016 (i.e., the 2015-2016 ENSO cycle) with a lead time of six months. Using the description in Section 2.4, dimension reduction is conducted using empirical orthogonal functions (EOFs), also referred to as spatial-temporal principal components (see Chapter 5 of Cressie and Wikle, 2011), on both

the input and response. The first 10 EOFs, which account for over 80% of the variability in the data, are retained for both the input and response. This same number of EOFs has been used in multiple previous SST applications (i.e., Berliner et al., 2000; Gladish and Wikle, 2014). Once again, the embedded input parameters are selected using the E-QESN model such that $\tilde{\tau} = 6$ and $m = 4$.

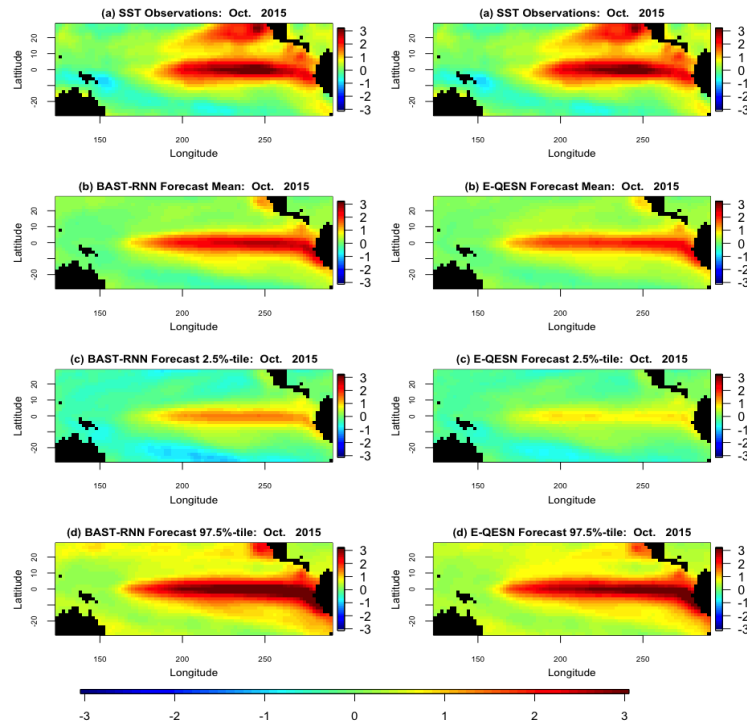


Figure 2: Spatial posterior summaries for all 2,229 oceanic spatial locations in the SST long-lead forecasting application for October 2015. The left column shows results from the BAST-RNN model, while the right column contains results from the competing E-QESN model for the same period. (a) The true SST for October 2015. (b) Posterior mean out-of-sample forecasts for the BAST-RNN model and mean out-of-sample forecasts over all ensembles for the E-QESN model. (c) Lower 2.5% P.I.s for the respective forecasting method. (d) Upper 97.5% P.I.s for the respective forecasting method.

Comparison of the forecasting ability of the BAST-RNN model and the E-QESN model for the entire spatial domain can be seen in Figure 1 for October 2015. Occurring directly before the peak of the 2015-2016 ENSO cycle (see Figure 3), October 2015 represents an important month from the most recent ENSO cycle. Overall, both methods pick up much of the warm intensity trend, with the BAST-RNN model forecasting a slightly higher inten-

sity (especially for the Niño 3.4 region) compared to the E-QESN method. Although both methods appear to produce P.I.'s with similar widths, the BAST-RNN model correctly indicates the possibility of a more intense warm event than the E-QESN model. Importantly, the highest intensity true values from the Niño 3.4 region for October 2015 are contained within the 95% P.I.'s for the BAST-RNN model. Furthermore, the BAST-RNN model is evaluated in terms of the previously described Niño 3.4 index in Figure 3. Much of the overall temporal nonlinear trend of the 2015-2016 ENSO cycle is captured by the BAST-RNN model, as shown in Figure 3, with all of the true values contained within the 95% P.I.'s. We should note, like the majority of other ENSO forecasting models, the forecast mean from the BAST-RNN model also underestimates the peak of the ENSO cycle.

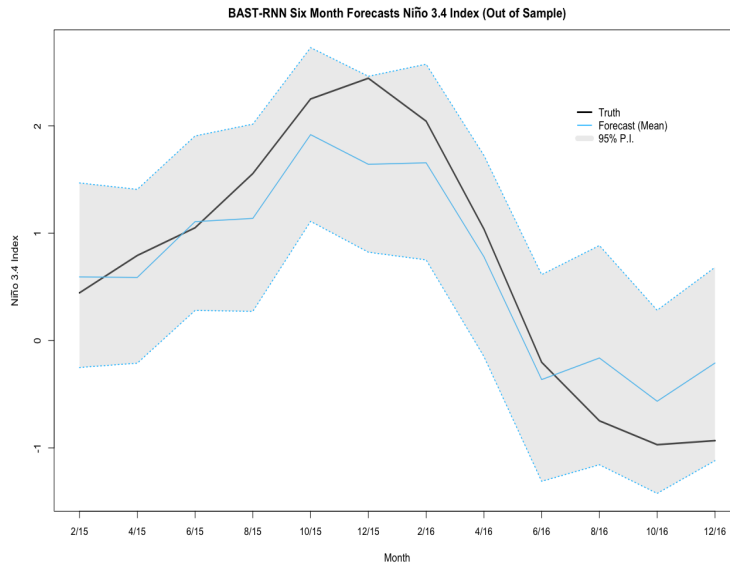


Figure 3: Summary of the posterior results with the BAST-RNN model for the Niño 3.4 index. For a given month, the Niño 3.4 index is defined as the average SST over all locations in the Niño 3.4 region (5°S - 5°N , 120° - 70°W). The solid black lines denotes the true Niño 3.4 index for a given month during the 2015-2016 cycle. Posterior mean out-of-sample forecasts from the BAST-RNN model are denoted by the light blue line. The grey shaded area represents the 95% P.I.s from the BAST-RNN for the Niño 3.4 index

Once again we evaluate the performance of the BAST-RNN against the three comparison models described above. Throughout the 2015-2016 ENSO cycle, Table 2 shows the BAST-RNN as a more accurate long-lead forecasting model than the other three models. Over the Niño 3.4 region, the BAST-RNN model greatly outperforms the other models, il-

illustrating the models ability to forecast nonlinear dynamics. Moreover, Table 2 also shows the BAST-RNN model having the lowest CRPS over all 2,229 locations in the application, thus providing useful uncertainty information across the entire spatial domain. By producing sensible uncertainty metrics, the BAST-RNN allows resource managers to make more informed decisions.

Model	Overall MSPE	Niño 3.4 MSPE	CRPS
BAST-RNN	0.247	0.188	3.387
E-QESN	0.288	0.261	3.722
GQN	0.304	0.686	-
Lin. DSTM	0.326	0.899	-

Table 2: Summary metrics for each of the four methods evaluated for the long-lead SST forecasting application. Overall MSPE denotes the MSPE calculated over all out-of-sample periods and all oceanic locations. The column Niño 3.4 MSPE denotes the MSPE over all locations in the Niño 3.4 region across all out-of-sample periods. The CRPS is calculated over all locations and out-of-sample time periods.

5 Discussion and Conclusion

The results of both applications presented above demonstrate the potential of using machine learning methods within a Bayesian modeling framework for forecasting nonlinear spatio-temporal processes. While many methods struggled with forecasting the 2015-2016 ENSO cycle, the BAST-RNN model forecasted much of the overall cycle correctly, especially when accounting for forecast uncertainty. Additionally, the BAST-RNN model was able to pick up the correct nonlinear trend for the multiscale Lorenz data despite a considerable amount of noise. With regards to both forecast accuracy and quantification of uncertainty, the BAST-RNN model was superior to the three competing models, over a reasonably long out-of-sample temporal span.

Placing popular machine learning methods, such as RNNs, within a more rigorous statistical framework allows for more thorough uncertainty quantification, while also providing a useful framework for building more complicated models. That is, the proposed BAST-RNN model provides a first-step towards more hierarchical machine learning methods that account for sources of variation at multiple levels. High-dimensional real-world processes often contain multiple layers of interconnected uncertainties, these uncertainties can more easily be untangled and formally modeled within the proposed modeling framework. Conversely, even the most precise uncertainty quantification methods are of diminishing value if they are not flexible enough to accurately forecast the process of interest. Thereby combining the forecasting ability of the RNN model, with the rigor of Bayesian modeling, the proposed methodology provides a powerful tool for modelers.

Critically, the proposed model can be used for a broad range of forecasting problems both within its current form and with relatively minor modification. For example, the model could easily be extended to account for different types of response data such as binary or count data. Moreover, the BAST-RNN is flexible enough to deal with varying degrees of nonlinearity, whereas past statistical nonlinear forecasting models may fail with higher levels of nonlinearity. The applications shown above provide evidence of this flexibility with the model producing accurate results for both a quasilinear process (SST) and a highly nonlinear process (Lorenz model).

Other extensions of the model include letting the parameters associated with the embedded input and the number of hidden units vary, which could more accurately account for the uncertainty associated with these choices. Putting the model within a fully Bayesian hierarchical framework is another possible extension. It is also likely that other forms of dimension reduction may be useful when considering the BAST-RNN model for other application. In particular, incorporating the nonlinearity or dynamics of the process explicitly in the selected dimension reduction method could be of use for future applications.

Acknowledgements

This work was partially supported by the U.S. National Science Foundation (NSF) and the U.S. Census Bureau under NSF grant SES-1132031, funded through the NSF-Census Research Network (NCRN) program.

References

- Barnston, A. G., He, Y., and Glantz, M. H. (1999), “Predictive skill of statistical and dynamical climate models in SST forecasts during the 1997?98 El Niño episode and the 1998 La Niña onset,” *Bulletin of the American Meteorological Society*, 80, 217–243.
- Barnston, A. G., Tippett, M. K., L’Heureux, M. L., Li, S., and DeWitt, D. G. (2012), “Skill of real-time seasonal ENSO model predictions during 2002–11: Is our capability increasing?” *Bulletin of the American Meteorological Society*, 93, 631–651.
- Belkin, M. and Niyogi, P. (2001), “Laplacian Eigenmaps and Spectral Techniques for Embedding and Clustering,” *MIPS*, 14.
- Berliner, L. M., Wikle, C. K., and Cressie, N. (2000), “Long-lead prediction of Pacific SSTs via Bayesian dynamic modeling,” *Journal of climate*, 13, 3953–3968.
- Carvalho, C. M., Polson, N. G., and Scott, J. G. (2010), “The horseshoe estimator for sparse signals,” *Biometrika*, 97, 465–480.
- Chandra, R. and Zhang, M. (2012), “Cooperative coevolution of Elman recurrent neural networks for chaotic time series prediction,” *Neurocomputing*, 86, 116–123.
- Chatzis, S. P. (2015), “Sparse Bayesian Recurrent Neural Networks,” in *Joint European Conference on Machine Learning and Knowledge Discovery in Databases*, Springer, pp. 359–372.
- Chien, J.-T. and Ku, Y.-C. (2016), “Bayesian recurrent neural network for language modeling,” *IEEE transactions on neural networks and learning systems*, 27, 361–374.
- Chorin, A. J. and Lu, F. (2015), “Discrete approach to stochastic parametrization and dimension reduction in nonlinear dynamics,” *Proceedings of the National Academy of Sciences*, 112, 9804–9809.

- Chung, J., Gulcehre, C., Cho, K., and Bengio, Y. (2015), “Gated feedback recurrent neural networks,” in *International Conference on Machine Learning*, pp. 2067–2075.
- Coifman, R. and Lafon, S. (2006), “Diffusion maps,” *Applied computational Harmonic Analysis*, 21, 5–30.
- Cressie, N. and Wikle, C. (2011), *Statistics for Spatio-Temporal Data*, New York: John Wiley & Sons.
- Crommelin, D. and Vanden-Eijnden, E. (2008), “Subgrid-scale parameterization with conditional Markov chains,” *Journal of the Atmospheric Sciences*, 65, 2661–2675.
- Fan, J. and Yao, Q. (2005), *Nonlinear time series*, Springer.
- Gan, Z., Li, C., Chen, C., Pu, Y., Su, Q., and Carin, L. (2016), “Scalable Bayesian Learning of Recurrent Neural Networks for Language Modeling,” *arXiv preprint arXiv:1611.08034*.
- George, E. I. and McCulloch, R. E. (1993), “Variable selection via Gibbs sampling,” *Journal of the American Statistical Association*, 88, 881–889.
- (1997), “Approaches for Bayesian variable selection,” *Statistica sinica*, 339–373.
- Ghosh, M., Maiti, T., Kim, D., Chakraborty, S., and Tewari, A. (2004), “Hierarchical Bayesian neural networks: an application to a prostate cancer study,” *Journal of the American Statistical Association*, 99.
- Gladish, D. W. and Wikle, C. K. (2014), “Physically motivated scale interaction parameterization in reduced rank quadratic nonlinear dynamic spatio-temporal models,” *Environmetrics*, 25, 230–244.
- Gneiting, T. and Katzfuss, M. (2014), “Probabilistic forecasting,” *Annual Review of Statistics and Its Application*, 1, 125–151.

- Graves, A. (2013), “Generating sequences with recurrent neural networks,” *arXiv preprint arXiv:1308.0850*.
- Green, P. J. (1995), “Reversible jump Markov chain Monte Carlo computation and Bayesian model determination,” *Biometrika*, 82, 711–732.
- Grooms, I. and Lee, Y. (2015), “A framework for variational data assimilation with superparameterization,” *Nonlinear Processes in Geophysics*, 22.
- Hobert, J. P. (2011), “The data augmentation algorithm: Theory and methodology,” *Handbook of Markov Chain Monte Carlo*, 253–293.
- Hu, S. and Fedorov, A. V. (2017), “The extreme El Niño of 2015–2016: the role of westerly and easterly wind bursts, and preconditioning by the failed 2014 event,” *Climate Dynamics*, 1–19.
- Jaeger, H. (2001), “The “echo state” approach to analysing and training recurrent neural networks-with an erratum note,” *Bonn, Germany: German National Research Center for Information Technology GMD Technical Report*, 148.
- Jan van Oldenborgh, G., Balmaseda, M. A., Ferranti, L., Stockdale, T. N., and Anderson, D. L. (2005), “Did the ECMWF seasonal forecast model outperform statistical ENSO forecast models over the last 15 years?” *Journal of climate*, 18, 3240–3249.
- L’Heureux, M. L., Takahashi, K., Watkins, A. B., Barnston, A. G., Becker, E. J., Di Liberto, T. E., Gamble, F., Gottschalck, J., Halpert, M. S., Huang, B., et al. (2016), “Observing and predicting the 2015-16 El Niño,” *Bulletin of the American Meteorological Society*.
- Liu, J. S. and Wu, Y. N. (1999), “Parameter expansion for data augmentation,” *Journal of the American Statistical Association*, 94, 1264–1274.

- Lorenz, E. N. (1963), “Deterministic nonperiodic flow,” *Journal of the atmospheric sciences*, 20, 130–141.
- (1996), “Predictability: A problem partly solved,” in *Proc. Seminar on predictability*, vol. 1.
- Lukoševičius, M. (2012), “A practical guide to applying echo state networks,” in *Neural networks: tricks of the trade*, Springer, pp. 659–686.
- Lukoševičius, M. and Jaeger, H. (2009), “Reservoir computing approaches to recurrent neural network training,” *Computer Science Review*, 3, 127–149.
- Ma, Q.-L., Zheng, Q.-L., Peng, H., Zhong, T.-W., and Xu, L.-Q. (2007), “Chaotic time series prediction based on evolving recurrent neural networks,” in *Machine Learning and Cybernetics, 2007 International Conference on*, IEEE, vol. 6, pp. 3496–3500.
- MacKay, D. J. (1992), “A practical Bayesian framework for backpropagation networks,” *Neural computation*, 4, 448–472.
- Matheson, J. E. and Winkler, R. L. (1976), “Scoring rules for continuous probability distributions,” *Management science*, 10, 1087–1096.
- McDermott, P. L. and Wikle, C. K. (2016), “A model-based approach for analog spatio-temporal dynamic forecasting,” *Environmetrics*, 27, 70–82.
- (2017), “An Ensemble Quadratic Echo State Network for Nonlinear Spatio-Temporal Forecasting,” *arXiv preprint arXiv:1708.05094*.
- Nair, V. and Hinton, G. E. (2010), “Rectified linear units improve restricted boltzmann machines,” in *Proceedings of the 27th international conference on machine learning (ICML-10)*, pp. 807–814.

- Ning, G., Zhang, Z., Huang, C., He, Z., Ren, X., and Wang, H. (2016), “Spatially supervised recurrent convolutional neural networks for visual object tracking,” *arXiv preprint arXiv:1607.05781*.
- O’Hara, R. B., Sillanpää, M. J., et al. (2009), “A review of Bayesian variable selection methods: what, how and which,” *Bayesian analysis*, 4, 85–117.
- Park, T. and Casella, G. (2008), “The bayesian lasso,” *Journal of the American Statistical Association*, 103, 681–686.
- Pascanu, R., Mikolov, T., and Bengio, Y. (2013), “On the difficulty of training recurrent neural networks,” in *International Conference on Machine Learning*, pp. 1310–1318.
- Richardson, R. A. (2017), “Sparsity in nonlinear dynamic spatiotemporal models using implied advection,” *Environmetrics*.
- Srivastava, N., Hinton, G. E., Krizhevsky, A., Sutskever, I., and Salakhutdinov, R. (2014), “Dropout: a simple way to prevent neural networks from overfitting.” *Journal of machine learning research*, 15, 1929–1958.
- Takens, F. et al. (1981), “Detecting strange attractors in turbulence,” *Lecture notes in mathematics*, 898, 366–381.
- Tang, B., Hsieh, W. W., Monahan, A. H., and Tangang, F. T. (2000), “Skill comparisons between neural networks and canonical correlation analysis in predicting the equatorial Pacific sea surface temperatures,” *Journal of Climate*, 13, 287–293.
- Tangang, F. T., Tang, B., Monahan, A. H., and Hsieh, W. W. (1998), “Forecasting ENSO events: A neural network–extended EOF approach,” *Journal of Climate*, 11, 29–41.
- Wikle, C. (2015), “Modern perspectives on statistics for spatio-temporal data,” *Wiley Interdisciplinary Reviews: Computational Statistics*, 7, 86–98.

- Wikle, C. K. and Hooten, M. B. (2010), “A general science-based framework for dynamical spatio-temporal models,” *Test*, 19, 417–451.
- Wilks, D. S. (2005), “Effects of stochastic parametrizations in the Lorenz’96 system,” *Quarterly Journal of the Royal Meteorological Society*, 131, 389–407.
- Wu, G., Holan, S. H., and Wikle, C. K. (2013), “Hierarchical Bayesian spatio-temporal Conway–Maxwell Poisson models with dynamic dispersion,” *Journal of agricultural, biological, and environmental statistics*, 18, 335–356.
- Yildiz, I. B., von Kriegstein, K., and Kiebel, S. J. (2013), “From birdsong to human speech recognition: Bayesian inference on a hierarchy of nonlinear dynamical systems,” *PLoS computational biology*, 9.

Appendix A: Specification of Priors

Below priors for all of the parameters in the BAST-RNN are detailed along with specific values for each of the hyper-parameters in the model.

Each element in the weight matrix \mathbf{W} is given the following prior distribution:

$$w_{i,\ell} = \gamma_{i,\ell}^w \text{TN}_{[-a_w, a_w]}(0, \sigma_{w,0}^2) + (1 - \gamma_{i,\ell}^w) \text{TN}_{[-a_w, a_w]}(0, \sigma_{w,1}^2) \quad \gamma_{i,\ell}^w \sim \text{Bernoulli}(\pi_w)$$

where $\sigma_{w,0}^2 = (1,000)^2$, $\sigma_{w,1}^2 = .005$, $a_w = .20$, and $\pi_w = .20$.

Each element in the weight matrix \mathbf{U} is given the following prior distribution:

$$u_{i,r} = \gamma_{i,r}^u \text{TN}_{[-a_u, a_u]}(0, \sigma_{u,0}^2) + (1 - \gamma_{i,r}^u) \text{TN}_{[-a_u, a_u]}(0, \sigma_{u,1}^2) \quad \gamma_{i,r}^u \sim \text{Bernoulli}(\pi_u)$$

where $\sigma_{u,0}^2 = (1,000)^2$, $\sigma_{u,1}^2 = .0005$, $a_u = .20$, and $\pi_u = .025$.

Each element in the weight matrix \mathbf{V}_1 is given the following prior distribution:

$$v_{1,k,i} = \gamma_{1,k,i}^v \text{Gau}(0, \sigma_{v_1,0}^2) + (1 - \gamma_{1,k,i}^v) \text{Gau}(0, \sigma_{v_1,1}^2) \quad \gamma_{1,k,i}^v \sim \text{Bernoulli}(\pi_{v_1})$$

where $\sigma_{v_1,0}^2 = 10$, $\sigma_{v_1,1}^2 = .01$, and $\pi_{v_1} = .50$.

Each element in the weight matrix \mathbf{V}_2 is given the following prior distribution:

$$v_{2,k,i} = \gamma_{2,k,i}^v \text{Gau}(0, \sigma_{v_2,0}^2) + (1 - \gamma_{2,k,i}^v) \text{Gau}(0, \sigma_{v_2,1}^2) \quad \gamma_{2,k,i}^v \sim \text{Bernoulli}(\pi_{v_2})$$

where $\sigma_{v_2,0}^2 = .5$, $\sigma_{v_2,1}^2 = .05$, and $\pi_{v_2} = .25$.

$$\begin{aligned} \boldsymbol{\alpha} &\sim \text{Gau}(\mathbf{0}, \sigma_\alpha^2 \mathbf{I}), \text{ where } \sigma_\alpha^2 = (.10)^2 & \boldsymbol{\mu} &\sim \text{Gau}(\mathbf{0}, \sigma_\mu^2 \mathbf{I}), \text{ where } \sigma_\mu^2 = 100 & \delta &\sim \text{Unif}(0, 1) \\ \sigma_\epsilon^2 &\sim \text{IG}(\alpha_\epsilon, \beta_\epsilon), \text{ where } \alpha_\epsilon = .001 \text{ and } \beta_\epsilon = .001. \end{aligned}$$

Appendix B: Derivation of Algorithm 1

Suppose we introduce the expansion parameter α where $\alpha = [\alpha_{i,\ell}]$ for $i = 1, \dots, n_h$ and $\ell = 1, \dots, n_h$, and $\alpha \subset \mathbf{A}$ where $\mathbf{A} \in \mathbb{R}^{n_h^2}$. Define the following function $t_\alpha : \mathbf{W} \rightarrow \mathbf{W}$. We require that t_α is a one-to-one differentiable function. We define Θ as all of the parameters in the model not associated with \mathbf{W} , such that $\Theta \equiv \{\mathbf{V}_1, \mathbf{V}_2, \boldsymbol{\mu}, \boldsymbol{\Gamma}_{V_1}, \boldsymbol{\Gamma}_{V_2}, \mathbf{U}, \boldsymbol{\Gamma}_U, \delta, \sigma_\epsilon^2\}$. Next, let $\mathbf{Y}_{1:T} \equiv \{\mathbf{Y}_1, \dots, \mathbf{Y}_T\}$ and $\tilde{\mathbf{X}}_{1:T} \equiv \{\tilde{\mathbf{X}}_1, \dots, \tilde{\mathbf{X}}_T\}$, with the notation $[\cdot]$ denoting a distribution, and we define the likelihood of the model (before the introduction of the expansion parameter matrix α) using the following slight abuse of notation $\prod_{t=1}^T [\mathbf{Y}_t \mid \Theta, \mathbf{W}, \boldsymbol{\Gamma}_W, \tilde{\mathbf{X}}_t] = [\mathbf{Y}_{1:T} \mid \Theta, \mathbf{W}, \boldsymbol{\Gamma}_W, \tilde{\mathbf{X}}_{1:T}]$. We assume that α is only dependent on $\Theta, \mathbf{W}, \boldsymbol{\Gamma}_W$, and $\mathbf{Y}_{1:T}$ through the transformation t_α and independent of these values otherwise.

The function t_α is defined as follows: $t_\alpha(\mathbf{W}) = [t_{\alpha_{i,\ell}}(w_{i,\ell})] = [\kappa(w_{i,\ell} - \alpha_{i,\ell})]$, where: $\kappa(q_\kappa) = -a + \frac{2a}{1+e^{-q_\kappa}}$, thus ensuring $q_\kappa \in [-a, a]$. The Jacobian for the transformation $t_\alpha(\mathbf{W})$, is defined as $J_\alpha(\mathbf{W}) = \frac{\partial}{\partial \mathbf{W}} t_\alpha(\mathbf{W}) = \prod_{i=1}^{n_h} \prod_{\ell=1}^{n_h} \frac{\partial t_{\alpha_{i,\ell}}(w_{i,\ell})}{\partial w_{i,\ell}}$.

Derivation of algorithm

1. Sample \mathbf{W} and $\boldsymbol{\Gamma}_W$ as follows:

$$[\mathbf{W}, \boldsymbol{\Gamma}_W \mid \Theta, \mathbf{Y}_{1:T}, \tilde{\mathbf{X}}_{1:T}] = \frac{[\Theta, \mathbf{W}, \boldsymbol{\Gamma}_W \mid \mathbf{Y}_{1:T}, \tilde{\mathbf{X}}_{1:T}]}{[\Theta \mid \mathbf{Y}_{1:T}, \tilde{\mathbf{X}}_{1:T}]} = \frac{\int_{\mathbf{A}} [\Theta, \mathbf{W}, \boldsymbol{\Gamma}_W, \alpha \mid \mathbf{Y}_{1:T}, \tilde{\mathbf{X}}_{1:T}] d\alpha}{[\Theta \mid \mathbf{Y}_{1:T}, \tilde{\mathbf{X}}_{1:T}]}$$

(These two equalities follow by definition.)

$$= \frac{\int_{\mathbf{A}} [\Theta, t_\alpha(\mathbf{W}), \boldsymbol{\Gamma}_W \mid \mathbf{Y}_{1:T}, \tilde{\mathbf{X}}_{1:T}] |J_\alpha(\mathbf{W})| [\alpha] d\alpha}{[\Theta \mid \mathbf{Y}_{1:T}, \tilde{\mathbf{X}}_{1:T}]}$$

(First we use the fact that α is not dependent on any other values in the model, before the transformation t_α is introduced. Then we transform \mathbf{W} , using the transformation t_α .)

$$= \int_{\mathbf{A}} [t_{\alpha}(\mathbf{W}), \Gamma_W \mid \Theta, \mathbf{Y}_{1:T}, \tilde{\mathbf{X}}_{1:T}] |J_{\alpha}(\mathbf{W})| [\alpha] d\alpha$$

(Follows by definition.)

Since we are actually interested in sampling \mathbf{W} , at this step we will use a change-of-variable so that we end up sampling \mathbf{W} instead. That is, suppose we call the value of $t_{\alpha}(\mathbf{W})$ sampled above, \mathbf{W}' , then transforming this value as $t_{\alpha}^{-1}(\mathbf{W}')$, we end up sampling \mathbf{W} . This results in step 1 of Algorithm 1 and defining α_0 as the simulated value from $[\alpha]$ leads to step 2.

2. Sample Θ and α , as follows:

$$[\Theta, \alpha \mid \mathbf{W}, \Gamma_W, \mathbf{Y}_{1:T}, \tilde{\mathbf{X}}_{1:T}] = \frac{[\Theta, \alpha, \mathbf{w}, \Gamma_W, \mathbf{Y}_{1:T}, \tilde{\mathbf{X}}_{1:T}]}{[\mathbf{w}, \Gamma_W, \mathbf{Y}_{1:T}, \tilde{\mathbf{X}}_{1:T}]}$$

(This follows by definition.)

$$= \frac{[\Theta, \alpha, t_{\alpha_0}^{-1}(\mathbf{w}), \Gamma_W, \mathbf{Y}_{1:T}, \tilde{\mathbf{X}}_{1:T}]}{[t_{\alpha_0}^{-1}(\mathbf{w}), \Gamma_W, \mathbf{Y}_{1:T}, \tilde{\mathbf{X}}_{1:T}]}$$

(For this step, we transform \mathbf{W} by using the transformation $t_{\alpha_0}^{-1}$ in the numerator and the denominator. Note, α_0 is defined above.)

$$\propto [\Theta, \alpha, \tilde{\mathbf{W}}, \Gamma_W, \mathbf{Y}_{1:T}, \tilde{\mathbf{X}}_{1:T}]$$

(In this step we are getting rid of the normalizing constant and defining $\tilde{\mathbf{W}} \equiv t_{\alpha_0}^{-1}(\mathbf{W})$, thus 3 step in Algorithm 1.)

$$= [\Theta, \alpha, t_{\alpha}(\tilde{\mathbf{W}}), \Gamma_W, \mathbf{Y}_{1:T}, \tilde{\mathbf{X}}_{1:T}] |J_{\alpha}(\tilde{\mathbf{W}})|$$

(Here we transform $\tilde{\mathbf{W}}$ with t_{α} and account for the corresponding Jacobian $J_{\alpha}(\tilde{\mathbf{W}})$.)

$$\propto [\mathbf{Y}_{1:T} \mid t_{\alpha}(\tilde{\mathbf{W}}), \Gamma_W, \Theta, \alpha, \tilde{\mathbf{X}}_{1:T}] [\Theta] [t_{\alpha}(\tilde{\mathbf{W}}) \mid \Gamma_W, \alpha] [\alpha] |J_{\alpha}(\tilde{\mathbf{W}})|$$

(Simply decomposing the joint distribution.)

Then the full conditionals for Θ and α are as follows:

$$[\alpha \mid t_{\alpha}(\widetilde{\mathbf{W}}), \Gamma_W, \Theta, \mathbf{Y}_{1:T}, \widetilde{\mathbf{X}}_{1:T}] \propto [\mathbf{Y}_{1:T} \mid t_{\alpha}(\widetilde{\mathbf{W}}), \Gamma_W, \Theta, \alpha, \widetilde{\mathbf{X}}_{1:T}] \\ \times [t_{\alpha}(\widetilde{\mathbf{W}}) \mid \Gamma_W, \alpha] [\alpha] |J_{\alpha}(\widetilde{\mathbf{W}})|$$

(Sample α using Metropolis-Hasting steps.)

$$[\Theta \mid t_{\alpha}(\widetilde{\mathbf{W}}), \Gamma_W, \alpha, \mathbf{Y}_{1:T}, \widetilde{\mathbf{X}}_{1:T}] \propto [\mathbf{Y}_{1:T} \mid t_{\alpha}(\widetilde{\mathbf{W}}), \Theta, \widetilde{\mathbf{X}}_{1:T}] [\Theta]$$

(Sample all of the parameters in Θ using Gibbs and Metropolis-Hasting steps.)

These two full conditionals lead directly to steps 4 and 6 of Algorithm 1, respectively, where $\mathbf{W}^* = t_{\alpha}(\widetilde{\mathbf{W}})$ and thus step 5 in Algorithm 1.